Comparing Pan-sharpened Landsat-9 and Sentinel-2 for Land-Use Classification Using Machine Learning Classifiers

Yassine Bouslihim[1,2] · Mohamed Hakim Kharrou[2] · Abdelhalim Miftah[3,4] · Taha Attou[2] · Lhoussaine Bouchaou[2,5] · Abdelghani Chehbouni[2,6]

Abstract

This paper evaluates the ability of two machine learning algorithms, Random Forest (RF) and Support Vector Machine (SVM), to generate land-use maps using the recently launched Landsat-9 and Sentinel-2, two of the most used and popular satellite imagery sources. The potential to improve Landsat-9 performance was tested by pan-sharpening different bands of high-resolution data (15 m). For optimal performance of both classifiers, model tuning methods were applied by trying different combinations of key parameters of each model. This comparison was made in two different areas in Central Morocco. The results show that SVM performs slightly better than RF in classifying two images. In addition, Sentinel-2 exhibits significant multivariety classification ability compared to the pan-sharpened Landsat-9, despite the improved resolution of the latter. Lastly, the best classification performances were recorded for the combination Sentinel-2/SVM classifier. At last, machine learning algorithms prove their efficiency in classifying satellite images with high performance.

Keywords Land-use classification · Landsat-9 · Sentinel-2 · Machine learning · Pan-sharpening

Background and Introduction

Land-use maps have become necessary for monitoring changes and managing land resources sustainably. However, such monitoring requires extensive effort, especially in large hardly accessible areas. Therefore, satellite images represent a valuable source of spatial data that can be used to provide helpful information and also investigate various spatial phenomena (Du et al. 2020; Ghasemloo et al. 2022) efficiently and rapidly (especially in the case of large areas) and cost-effectively (Huyck et al. 2014). Furthermore, the development of satellites was accompanied by the evolution of many algorithms used for satellite image classification, retrieving a set of spatial information or using them as input to predict a specific parameter or phenomenon (Lary et al. 2018). The classification of satellite images to obtain land-use land-cover (LULC) maps is one of the most important applications that combine satellite images and algorithms (Talukdar et al. 2020). The demand for such maps has become significant due to their importance in natural resource management (Bouslihim et al. 2021a; Kala and Kumar 2022; Montalván-Burbano et al. 2021). Also, it helps to understand the impact of human activities on the ecosystem (Berihun et al. 2021) or to be used to understand the distribution of another parameter or phenomenon (Aouichaty et al. 2022; John et al. 2022). Therefore, extracting this type of information requires either the application of unsupervised classification methods without relying on samples or reference areas (Alshari and Gawali 2021; Georganos et al.

✉ Yassine Bouslihim
  yassine.bouslihim@gmail.com

[1] National Institute of Agricultural Research (INRA), CRRA, Tadla, Morocco

[2] International Water Research Institute (IWRI), Mohammed VI Polytechnic University (UM6P), Lot 660, Hay Moulay Rachid, 43150 Ben Guerir, Morocco

[3] Faculty of Sciences and Techniques, Laboratory Physico-Chemistry of Processes and Materials, Hassan First University of Settat, Settat, Morocco

[4] Faculty of Science and Techniques, Laboratory of Intelligent Systems Georesources and Renewable Energies, Sidi Mohamed Ben Abdellah University, Fes, Morocco

[5] Laboratory of Applied Geology and Geo-Environment, Ibn Zohr University, 80035 Agadir, Morocco

[6] Center for Remote Sensing Applications (CRSA), Mohammed VI Polytechnic University (UM6P), Lot 660, Hay Moulay Rachid, 43150 Ben Guerir, Morocco

2018) or the supervised classification methods. The latter is based mainly on representative samples from all groups of interest (e.g., land-use type) in order to classify the values of individual image components (pixel), including spectral reflectance or grayscale values (Nagne et al. 2019; Shaharum et al. 2018).

Htitiou et al. (2019) evaluated the feasibility of phenological data extracted from Sentinel-2 and Landsat-8 using the Random Forest (RF) model. They reported a high accuracy for Sentinel-2 for crop classification in irrigated areas in Morocco. Van Leeuwen et al. (2020) used three different algorithms (RF, Support Vector Machine (SVM), and Artificial Neural Network (ANN)) to produce a LULC map from Sentinel-2 on temporarily inundated areas (Hungary). Results show a high accuracy with slight differences between the three models. Ghayour et al. (2021) compared the performances of five models to generate LULC in western Iran. They report that the SVM model has the highest overall accuracy (OA) for satellite data and more accurate performance for Sentinel-2 than Landsat-8. Results also show that Maximum Likelihood Classification (MLC) and Minimum Distance (MD) models provided the lowest accuracy. In another study from Vietnam, Thanh Noi and Kappas (2017) used Sentinel-2 with three models (RF, SVM, and K-Nearest Neighbor (KNN)) and 14 different sizes of training samples. Results show a high accuracy for all classifications with a slight superiority of SVM. Karan and Samadder (2018) evaluated the performance of six classification techniques to extract land-use maps from the WorldView-2 satellite in India. Results show that only two classifiers (SVM and ANN) produced good results. Other classifiers, such as MLC, MD, and Spectral Angle Mapper, had not produced satisfactory results. All these studies use different satellites and a variety of classification algorithms. Although the findings of these studies are very diverse, overall, they all concur that the SVM model has high accuracy.

This new mission, Landsat-9, is a continuation of efforts to study and understand our planet since the launch of the first Landsat image in 1972. This Landsat-9 satellite has joined its sibling, the Landsat-8 satellite, in orbit, permitting the acquisition of images every eight days. Landsat 9 transmits 14-bit data from OLI-2, which provides a better view of darker areas, such as forests and coastal waters, than the 12-bit data from Landsat 8 OLI. This enhancement in radiometric resolution can also be supported by an additional improvement in spatial resolution based on pan-sharpening methods, which might contribute significantly in object detection and classification.

In the present study, we aim to assess the ability of the recently launched Landsat-9 satellite compared to Sentinel-2 for generating land-use maps based on two of the most popular classification algorithms (RF and SVM). The Landsat-9 images were pan-sharpened to a resolution comparable to that of Sentinel-2. This work was performed in a first area characterized by an urban trend surrounded by agricultural land and a rural area characterized by agricultural land and the Oum Rabii river. This study will help explore the new Landsat-9 product, especially the pan-sharpening effect on land-use map production.

Materials and Methods

Site Description

Two study areas of different characteristics were chosen, each occupying 227 km^2 (Fig. 1). The first area (zone 1) represents Settat town in the Casablanca-Settat region, Morocco. This zone has an urban character with diverse land use; for example, we can find some forest areas in the North of the town, surrounded by agricultural and pasture lands. The second area (zone 2) represents a part of Bni Chegdale commune, Fquih Ben Salah province. This area has a rural character with randomly distributed habitats and crop circles; these parcels are irrigated from the Oum Rabii river (located south of the area). In the present study, considering the specificity of each site and for classification purposes, the two areas were combined and considered as a single area to ensure the presence of a variety of land-use types.

Image Processing

Spatial remote sensing is increasingly helpful for LULC mapping in large or hard-to-access areas, using spectral bands from different electromagnetic spectrum wavelengths. However, LULC classification requires high-resolution images of the Earth's surface, which are not always available. This work compares the performance and evaluates the feasibility of using high-resolution multispectral images for land-use classification. For this purpose, two free-access satellite products with 0% cloud cover were used (Table 1).

Landsat-9 is a sun-synchronous satellite launched on September 27, 2021, and the images were made available for download in February 2022, resulting in a collaboration between NASA and the United States Geological Survey (USGS). It has an OLI-2 (Operational Land Imager) sensor to capture multispectral images in the visible and near-medium infrared wavelengths and a TIRS-2 (Thermal Infrared Sensor) spectrometer to study the ground temperature. Data from the new Landsat-9 sensor have important technological characteristics regarding spectral resolution, signal quantification level, signal-to-noise ratio, and radiometric resolution (14 bits), compared to the 12 bits for Landsat-8 and the 8-bit resolution for Landsat-7. Therefore, Landsat-9 provides better radiometric signal measurement sensitivity than previous Landsat missions. Furthermore, it improves
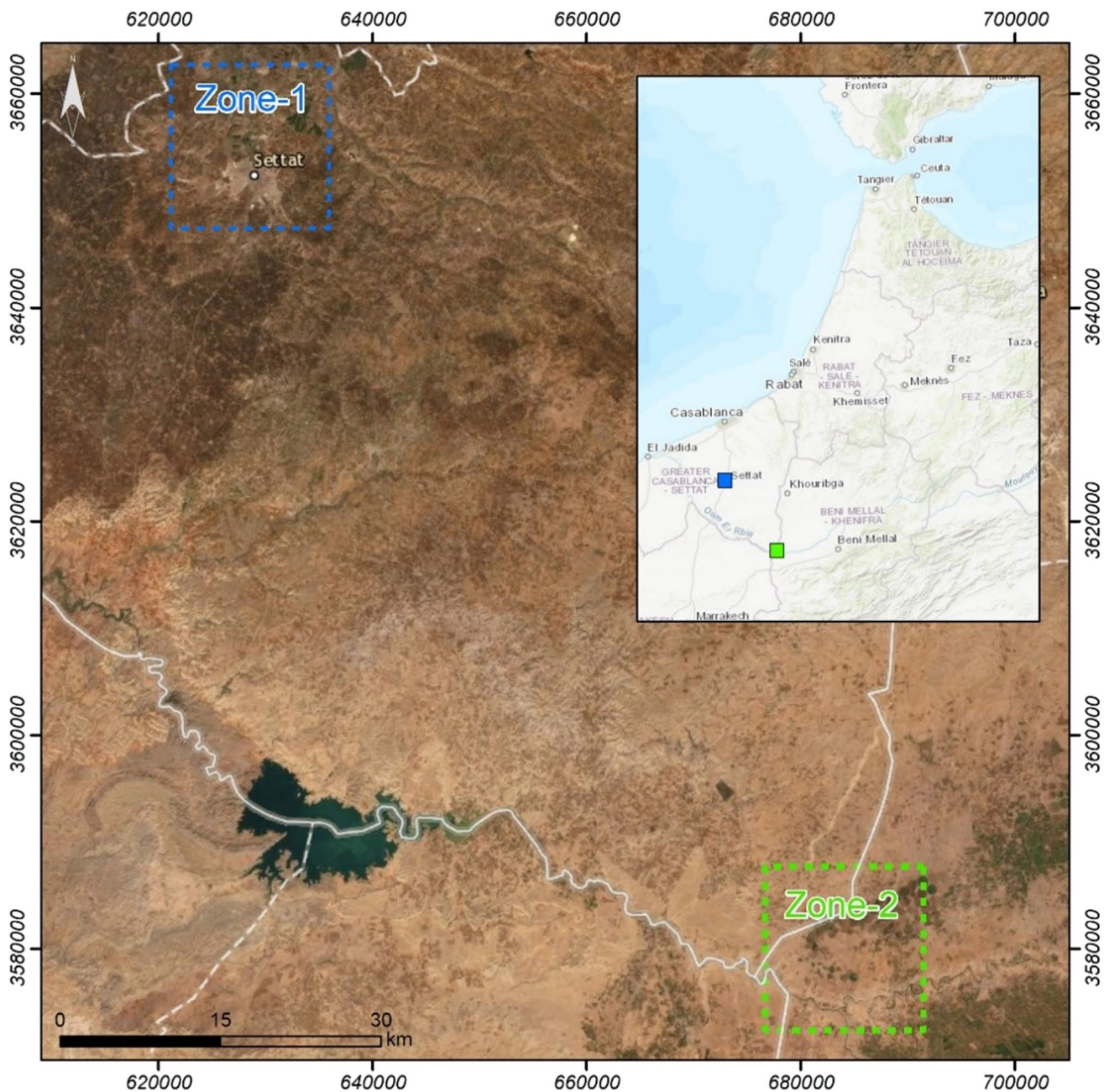
Fig. 1 Geographical location of selected study areas

change recognition, especially in darker areas such as water or dense forest (U.S. Geological Survey 2019).

Two satellite images of the same scene were downloaded from the USGS website (https://earthexplorer.usgs.gov/), captured in the daytime to enable maximum solar irradiation of the Earth's surface. Landsat-9 data are delivered at L2SP and L1TP correction levels from the T1 collection 2 with a UTM 29 N projection. The spectral bands from visible (blue, green, and red), near infrared (NIR), and shortwave infrared (SWIR1 and SWIR2) of the atmospherically corrected L2SP level with a spatial resolution of 30 m have been layer stacked. These data were spatially enhanced by the panchromatic band of the L1TP level with a resolution of 15 m to increase the Landsat-9 sensor data resolution.

The BROVEY pan-sharpening algorithm (Eqs. 1 and 2) was used for the Landsat-9 bands (Gillespie et al. 1987; Johnson et al. 2012). This algorithm allows the fusing of data from different sensors. It is based on the chromatic transformation of spectral bands that relies on the normalization of the bands from the low-resolution multispectral (MS)

Table 1 Landsat-9 and Sentinel-2's main characteristics

Sensor	Bands	Spectral range (μm)	Pixel size (m)	Spectral resolution	Radio-metric resolution (bit)	Revisit time (days)	Granule ID	Cloud cover (%)	Acquisition time
Landsat-9	Band 1-coastal/aerosol	0.433–0.453	30	11 bands	16	16	LC09_L2SP_202037_20220114_2 0220116_02_T1	0.08	2022–01–14 11h03min 59 s
	Band 2-blue	0.450–0.515	30				LC09_L1TP_202037_20220114_2 0220114_02_T1		
	Band 3-green	0.525–0.600	30						
	Band 4-red	0.630–0.680	30						
	Band 5-NIR	0.845–0.885	30						
	Band 6-SWIR 1	1.560–1.660	30						
	Band 7-SWIR 2	2.100–2.300	30						
	Band 8-panchromatic	0.500–0.680	15						
	Band 9-cirrus	1.360–1.390	30						
	Band 10-TIRS 1	10.30–11.30	100						
	Band 11-TIRS 2	11.50–12.50	100						
Sentinel-2	Band 1-coastal	0.433–0.453	60	13 bands	12	5	S2A_MSIL1C_20220116T111411_ N0301_R137_ T29SPR_20220116T131348	0	2022–01–16 11 h 14 min 11 s
	Band 2-blue	0.457–0.522	10				S2A_MSIL1C_20220116T111411_ N0301_R137_ T29SPS_20220116T131348		
	Band 3-green	0.542–0.577	10						
	Band 4-red	0.650–0.680	10						
	Band 5-veg red	0.679–0.718	20						
	Band 6-veg red	0.732–0.747	20						
	Band 7-veg red	0.773–0.793	20						
	Band 8-NIR	0.784–0.899	10						
	Band 8A-veg red	0.855–0.885	20						
	Band 9-water v	0.935–0.955	60						
	Band 10-cirrus	1.36–1.39	60						
	Band 11–SWIR 1	1.565–1.655	20						
	Band 12–SWIR 2	2.10–2.28	20						

image and are subsequently multiplied by the panchromatic (PAN) image to obtain a high spatial resolution multispectral (MSpan) image (Wang et al. 2005; Liu and Moore 1998; Zhang 1999):

$$MS_{pan} = \frac{MS * PAN}{I} \qquad (1)$$

$$I = \frac{(0.42 * Blue + 0.98 Green + 0.6 * Red)}{2} \qquad (2)$$

where I is intensity which is a function of multispectral bands.

The BROVEY pan-sharpening algorithm can produce spectral distortions in the bands used in the classification. We have chosen this algorithm after testing several others based on previous works proving that it effectively improves spatial resolution. In the present work, no spectral distortions were observed in the bands after pan-sharpening.

Sentinel-2 is also a sun-synchronous satellite, placed in orbit since 2015 by the European Space Agency and developed under the Copernicus program. Sentinel-2 products are characterized by systematic observations on a global scale of multispectral images of high spatial and temporal resolution

(Table 1). They are widely used in mapping and monitoring detail phenomena, such as detecting spatio-temporal variations in land cover, geochemical/physical variation, vegetation cover, and natural disaster management (Kollert et al. 2021; Ibrahim et al. 2018).

Two images were downloaded from the ESA website (https://scihub.copernicus.eu/) and captured on a very close date to Landsat-9. These data are distributed at the L1C level (top of atmosphere reflectance) with the same global geodetic system as the other data used. The Sentinel-2 images used in this study were acquired under clear sky conditions. The nearest neighbor resampling algorithm was used to unify the spatial resolution of band-2 to 8A, band-11, and band-12. This downscaling procedure improves classification accuracy (Atkinson 2013). The bands used for each image have been marked in bold in Table 1.

Presentation of Classifiers and Training/Testing Dataset

Two well-known machine learning algorithms were tested to evaluate their capability for land-use mapping based on Sentinel-2 and pan-sharpened Landsat-9 images. Random

Forest (RF) (Breiman 2001) and Support Vector Machine (SVM) (Meyer and Wien 2015) algorithms have been used extensively to solve classification and regression problems. These models have been applied to several fields, such as discrimination of species composition types (Crabbe et al. 2020), digital soil mapping (Bouslihim et al. 2021b), and crop classification (Fu et al. 2021).

Classification model development requires data representing various land-use classes for training and evaluating classification results. In the present study, we have focused on six classes: agriculture, pasture, forest, water, bare soil, and urban. Sample collection was done by field surveys using GPS (Global Positioning System). In addition, a second validation was done based on Google Earth orthorectified images to verify the quality and position of the samples. Furthermore, samples were collected as points for spatially limited classes (water and forest) or surfaces (polygons) for large surface classes. Figure 2 represents the geographical location of samples used for model training and testing (validation). However, collected samples were not equally sized due to the limited presence of particular classes such as water and forest. To avoid this inequality, we homogenized training samples before model tuning using the minimal value class. Then, 260 samples for each land-use class (1560 samples in total) were used for the RF and SVM model tuning and development.

Classification Accuracy

Classification performances can be checked by a visual control to assess the consistency of the obtained classification with the distribution of the different classes. Also, a statistical verification can be performed based on a confusion matrix and other statistical indices such as precision, recall, and f1 score for model performances in each land-use class. The macro-averaged f1 score, the overall accuracy (OA), and the Kappa coefficient were also used to assess the general model performance. Therefore, 100 independent samples for each land-use class (600 in total) were used to evaluate the classification performance for both models.

Results

Spectral Reflectance Analysis

Spectral reflectance of different classes, including forest, agriculture, pasture, urban, bare soil, and water, was extracted to examine and compare Landsat 9 and Sentinel-2 sensors (Figs. 3 and 4).

Figure 3 shows the spectral reflectance distribution of training pixels for the pan-sharpened Landsat-9 and Sentinel-2 bands. In all bands, several outliers for the urban area
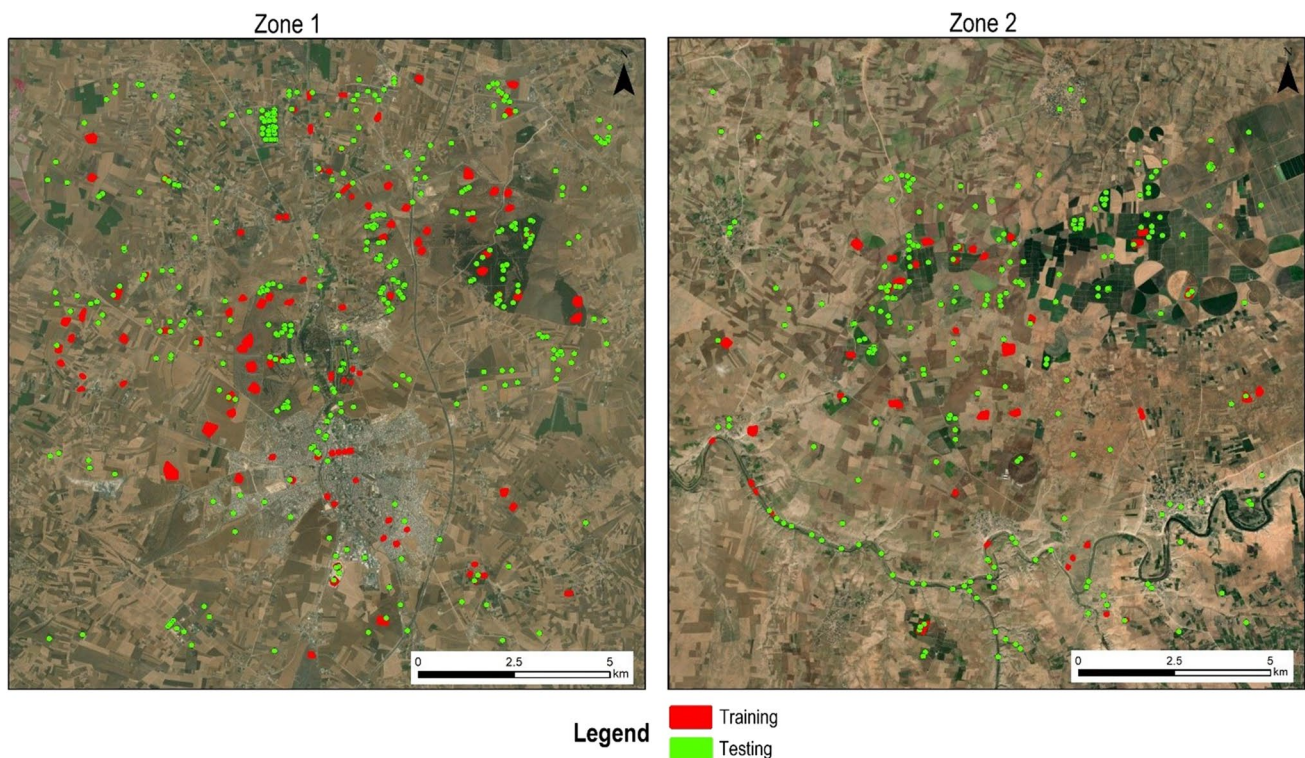

Fig. 2 Distribution of training and testing samples

Fig. 3 Spectral reflectance distribution for training data of different land-use classes across pan-sharpened Landsat-9 (top) and Sentinel-2 (below)
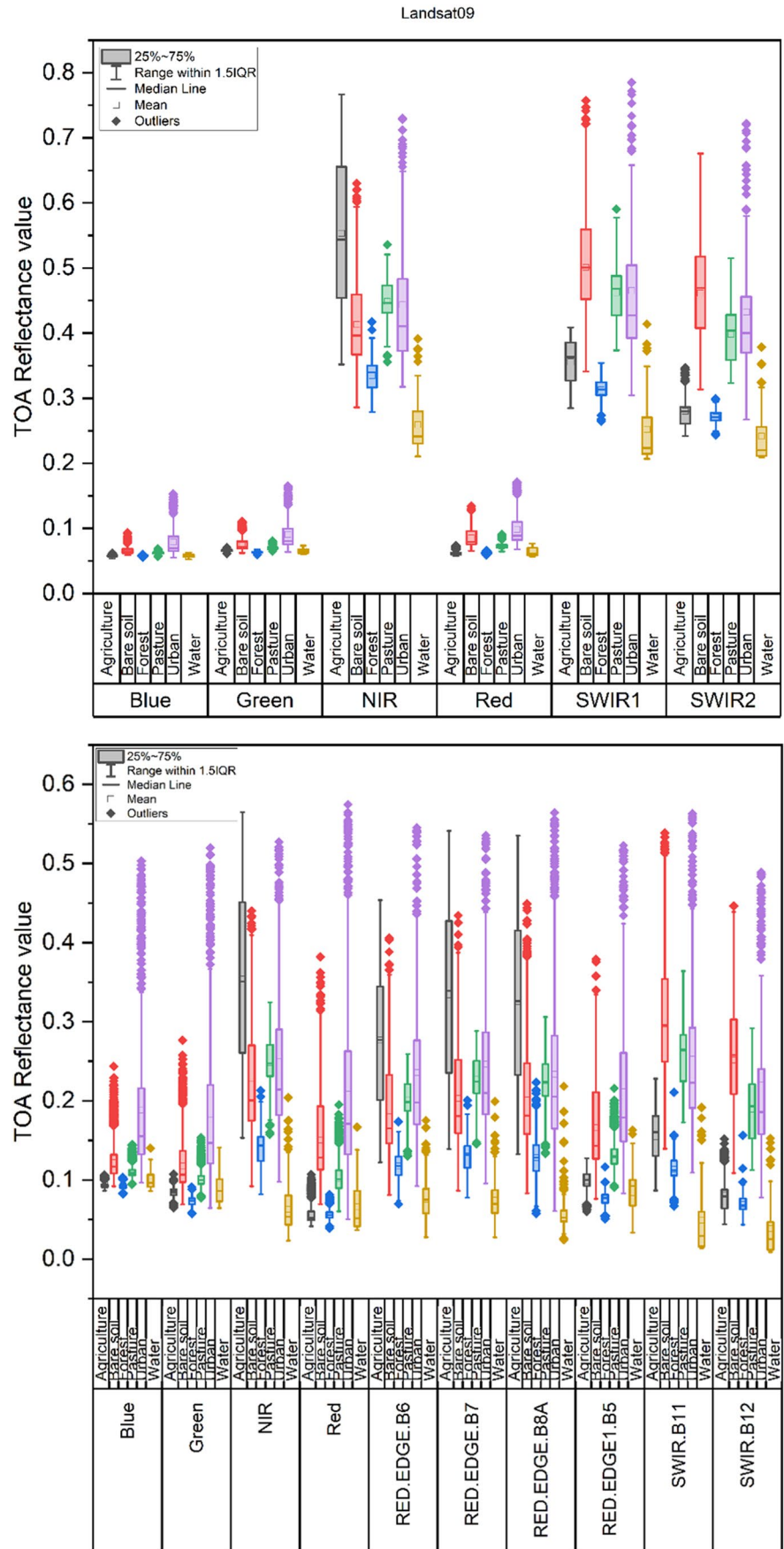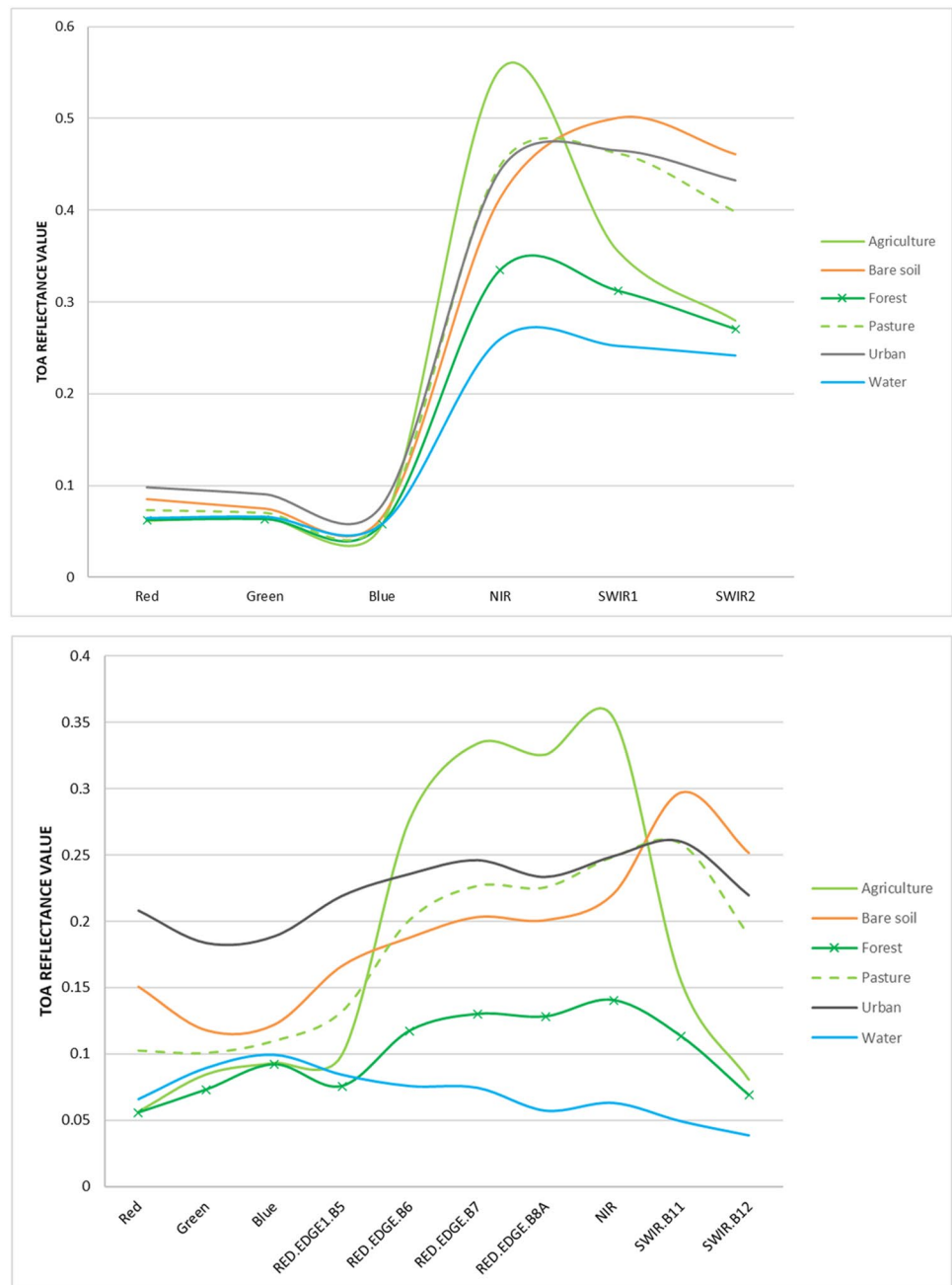
Fig. 4 Spectral reflectance curves for training data of different land-use classes across pan-sharpened Landsat-9 (top) and Sentinel-2 (below)

are detected for the first one, followed by bare soil (except for SWIR2) and a few outliers for water at NIR, SWIR1, and SWIR2. Overall, agriculture, forest, and water reflectance are significantly distinguishable from the other classes, especially at NIR, SWIR1, and SWIR2. For the Sentinel-2 image, we observe the presence of outliers for most classes in all available bands. As in the case of Landsat-9, the reflectance of agriculture, bare soil, and water is different from the other classes, especially in the NIR, B6, B7, B8A, and SWIR.B11 bands.

In Fig. 4a (pan-sharpened Landsat-9), the different classes show approximately the same spectral variation for the selected bands. A generally decreasing spectral response in the visible bands can be observed. In addition, a significant increase in reflectance was detected in the NIR range, with the highest value for agriculture records. For the SWIR range, the forest and agriculture show a decrease in reflectance, whereas the other classes (urban, pasture, and bare soil) keep a high spectral response. The water class is characterized by the lowest reflectance in the NIR and SWIR range of the Landsat-9 sensor. Figure 4b (Sentinel-2) shows a large spectral difference, with high spectral separability represented by non-identical reflectance curves from the RED-EDGE to SWIR bands.

Agriculture and water always show high and low values in the RED-EDGE.B6 to B8A and NIR, respectively. The reflectance curves are different because of the spectral characteristics of both sensors. The number and spectral range of the bands used, which vary from visible to SWIR, are different. As shown in Table 1, the Sentinel sensor has ten bands, while Landsat has only six bands. The wavelengths also vary; for example, the blue band varies between 0.450 and 0.515 μm for Landsat-9 and between 0.457 and 0.522 μm for Sentinel 2, thus resulting in different reflectance values for each class. Regarding the similarity of the spectral signatures of water and vegetation, we have reported this in the manuscript. Some sampling points were located in areas affected by an algal bloom, causing a green coloration of water, which leads to a slight spectral confusion between vegetation and water.

The obtained results show that the Landsat-9 and Sentinel-2 sensors generally have the same spectral changes but with more details for Sentinel-2 characterized by its high resolution, which could be a crucial factor in the reliability and accuracy of classification results. It will be difficult for the Landsat-9 sensor to distinguish between classes because of their almost identical spectral signatures.

Classifiers Model's Development

Optimal parameters for model development must be carefully chosen to achieve the best results for the machine learning algorithms. Therefore, two essential parameters must be tuned for the RF model: the *mtry* and *ntree*, whereas *cost*, *gamma*, and kernel function type are the parameters that usually influence the results of the SVM classifier. Model tuning was performed in the present study to facilitate the selection of the optimal parameters for each model. Furthermore, for RF classifier, a *ntree* of 500 with a *mtry* of 2 and 6 was found to be the optimal value for Landsat-9 and Sentinel-2, respectively. While the best SVM model was obtained from a radial model, *gamma* of 0.5, with a *cost* of 256 and 128 for Landsat-9 and Sentinel-2, respectively.

Land-Use Classification Results

The best models for RF and SVM were used to generate a distribution map of the different land-use classes. The two areas (zone 1 and zone 2) were combined for a more manageable representation of the results. Table 2 represents the surface and the percentage of the six classes obtained by pan-sharpened Landsat-9 and Sentinel-2 classification using RF and SVM classifiers. Generally, bare soil occupies over half of the total area; pasture takes the second position, followed by the urban area, agriculture, forest, and water, which occupies a small surface.

A few important observations were made by comparing classification results. The surface of the water body identified by pan-sharpened Landsat-9 + SVM was significantly larger (3.5 km^2), about three times the water estimated by the other classifications. Similarly, the urban area for the pan-sharpened Landsat-9 + SVM combination is the largest with 30.8 km^2, and the Sentinel-2 + RF captured a smaller area than the others (24.8 km^2). Regarding pasture areas, the classifications obtained by RF (for both images) gave lower values (144.5–147.2 km^2) compared to SVM (151.4–153.1 km^2). The forest area captured by Sentinel-2 + SVM is larger than the three other classifications, with 7.8 km^2. For agricultural areas, the Sentinel-2 + SVM captured the smallest area (22.7 km^2), while the pan-sharpened Landsat-9 + RF captured an area of 27.6 km^2. For the last class, the bare soil captured by RF is larger than SVM, with 247.4 and 249.7 km^2 for pan-sharpened Landsat-9 and Sentinel-2, respectively. The SVM classifier captured smaller areas, with 237.5 km^2 for pan-sharpened Landsat-9 and 243 km^2 for Sentinel-2.

Figures 5 and 6 show the land-use classification obtained from the pan-sharpened Landsat-9 and Sentinel-2, respectively. The overall visual control shows a similarity between all classification outputs for both models. For zone 1, we can observe the excellent recognition of numerous roads, especially the highway that crosses the whole area and other secondary roads distributed across the entire zone. Also, the small water surface in the North of zone 1 (basins of the

Table 2 Comparison of the occupied area of different classes

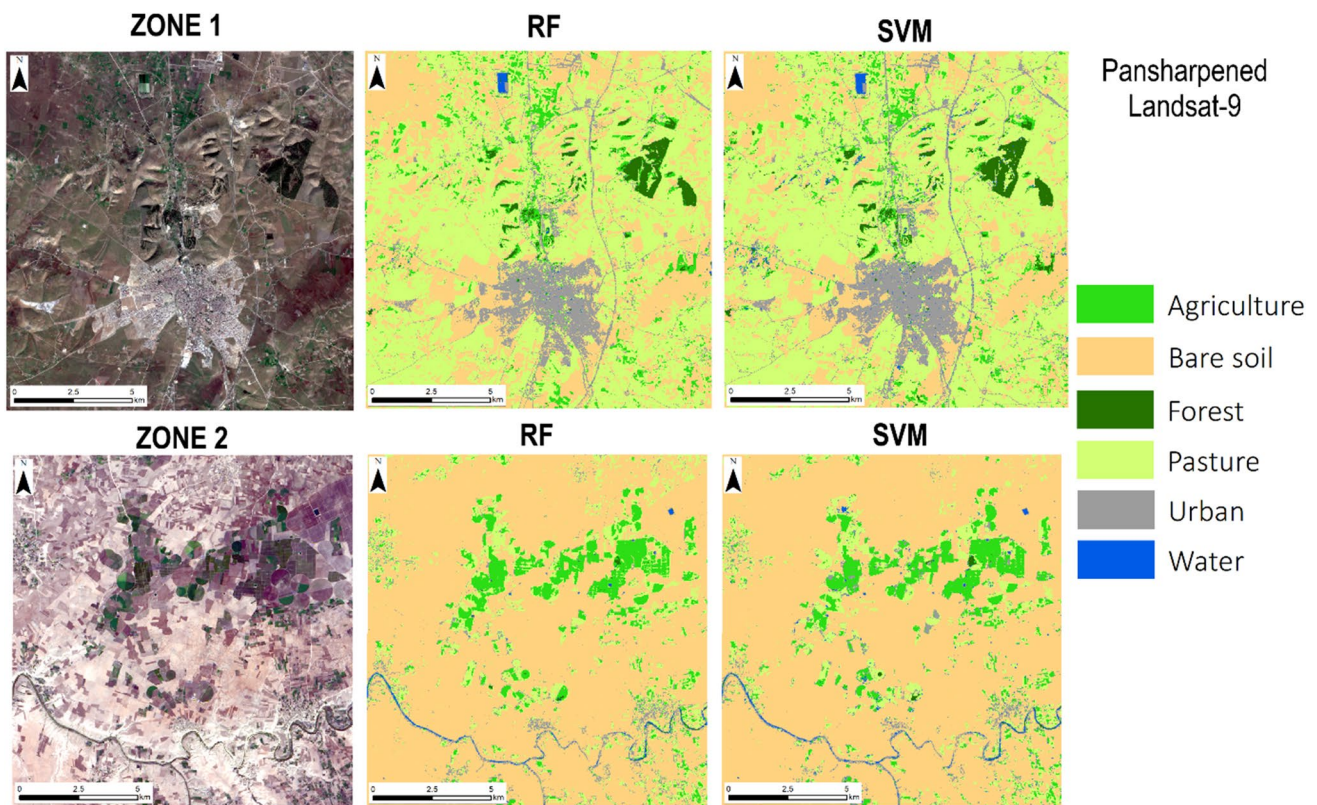|	Sentinel-2				Pan-sharpened Landsat-9			
	RF		SVM		RF		SVM	
	Surface (km^2)	%	Surface (km^2)	%	Surface (km^2)	%	Surface (km^2)	%
Agriculture	25.8	5.7	22.7	5.0	27.6	6.1	25.0	5.5
Bare soil	249.7	55.0	243.0	53.5	247.4	54.5	237.5	52.3
Forest	5	1.1	7.8	1.7	4.8	1.0	5.8	1.3
Pasture	147.2	32.4	153.1	33.7	144.5	31.8	151.4	33.3
Urban	24.8	5.5	26.2	5.8	28.7	6.3	30.8	6.8
Water	1.5	0.3	1.2	0.3	1.1	0.3	3.5	0.8

Fig. 5 Land-use maps obtained from the pan-sharpened Landsat-9 image

water treatment station of Settat town) was well identified in the four maps along with the surface occupied by the forest in the North-East.

Regarding zone 2, we can notice that the main river was clearly detected, with a few small water bodies distributed in zone 2 (irrigation water storage basins). However, some agricultural areas were misclassified as forests for Sentinel-2 + SVM.

The visual control made at a higher scale allows better analysis and comparison of classification results. Figure 7 presents the geographical location of the six selected classified areas. In Fig. 8A, we focused on water basins of the wastewater treatment station of Settat town. It can be noticed that the combination Sentinel-2 + RF was the only classifier capable of identifying the basin on the bottom right as a water area. In contrast, the different other combinations classified it as an urban area. Also, using both classifiers, a group of small basins located below the wastewater treatment station was only identified in the Sentinel-2 image. Besides, a small area of agriculture in the northeast corner was misclassified as forest (by the Sentinel-2 + SVM). The previous results are valid for the second case (Fig. 8B). The forest was identified in a similar pattern. However, misclassification of the road in the northwest corner was observed in the pan-sharpened

Landsat-9 + SVM, where some pixels were classified as water. In the case of Fig. 8C, two observations can be made: (i) pixels classified as forest are very frequent in images classified by SVM, and (ii) the small lake located in the center of the image was well captured in the case of Sentinel-2 + RF.

Moreover, the two roads on the left were well classified in the case of the Sentinel-2. The classification results for the example shown in Fig. 8D are generally similar. The river path was well captured in the different combinations. The only apparent difference was that more pixels were classified as urban in Landsat-9 than in Sentinel-2. In Fig. 8E, water collection basins were well captured along with most agricultural areas. However, two important observations should be noted; agricultural lands were classified as forests by Landsat-9 + RF, Landsat-9 + SVM, and Sentinel-2 + SVM. And other agricultural or pasture lands were classified as urban. The only correct classification was observed in the Landsat-9 + RF combination.

Regarding Fig. 8F, a misclassification of some bare soil areas classified as forest areas was observed in the Sentinel-2 + SVM combination. Many different areas were classified as urban in the same classification. In addition, we can note that in the Landsat-9 + SVM case, another area was classified as water, even though it does not exist.
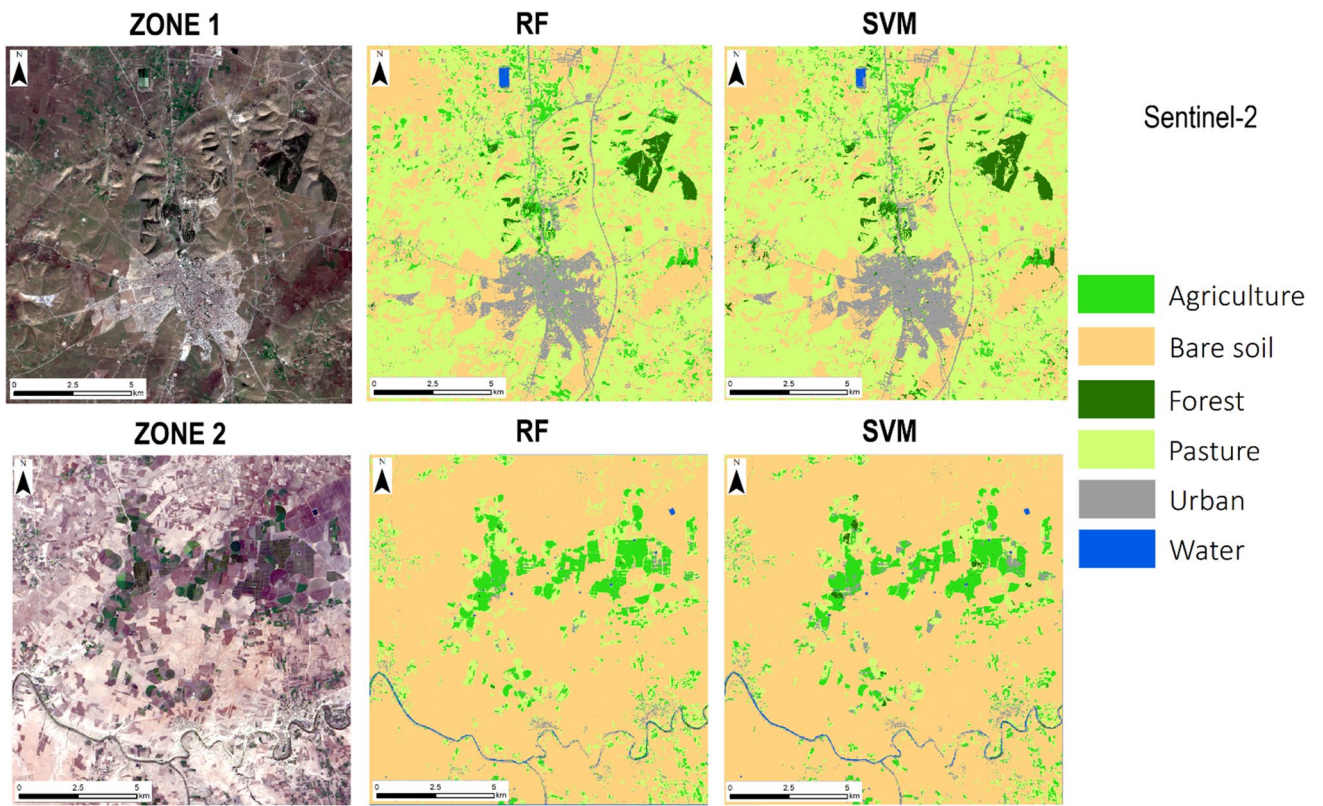
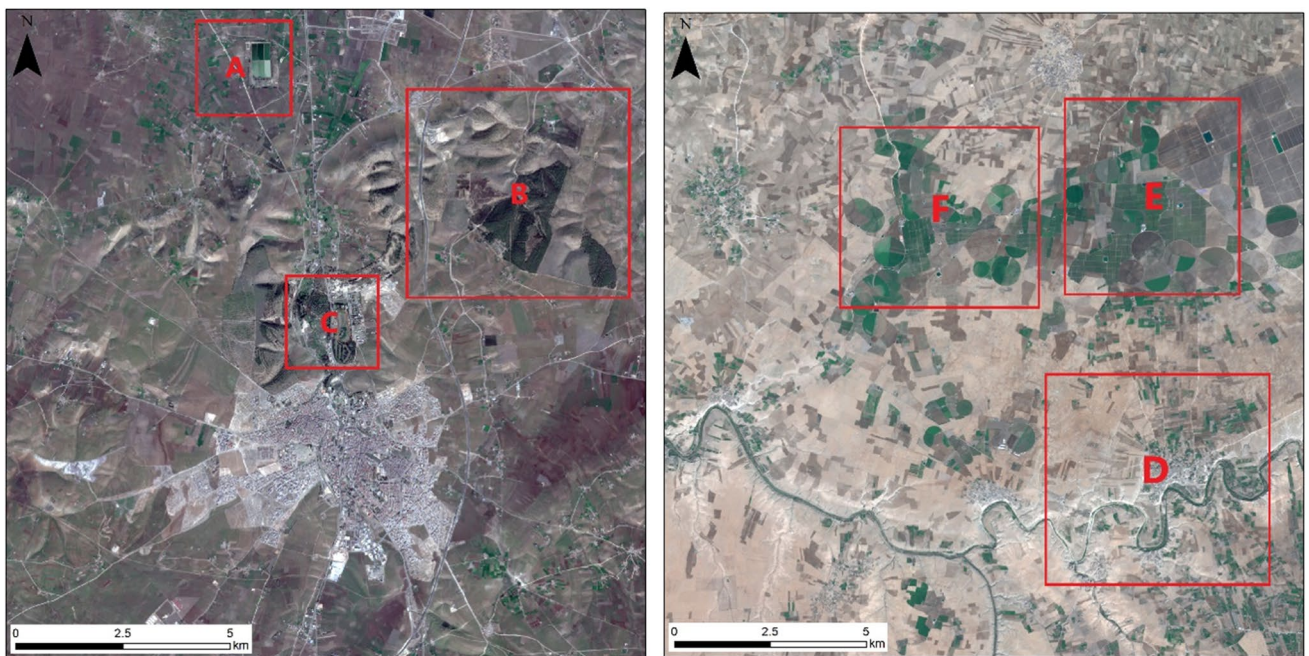**Fig. 6** Land-use maps obtained from the Sentinel-2 image

Fig. 7 Distribution of different selected areas

Fig. 8 A series of frames showing the comparison of different classification results
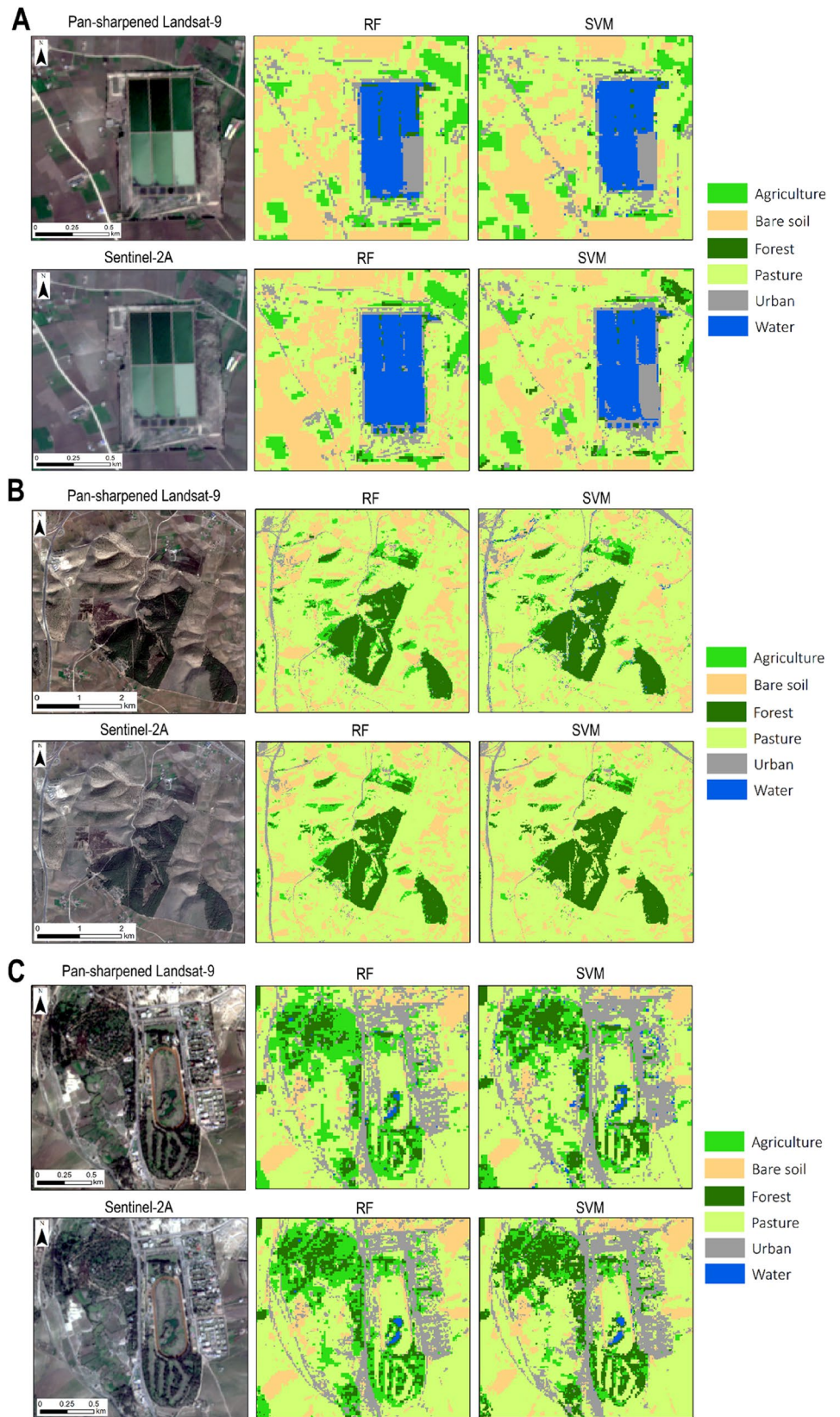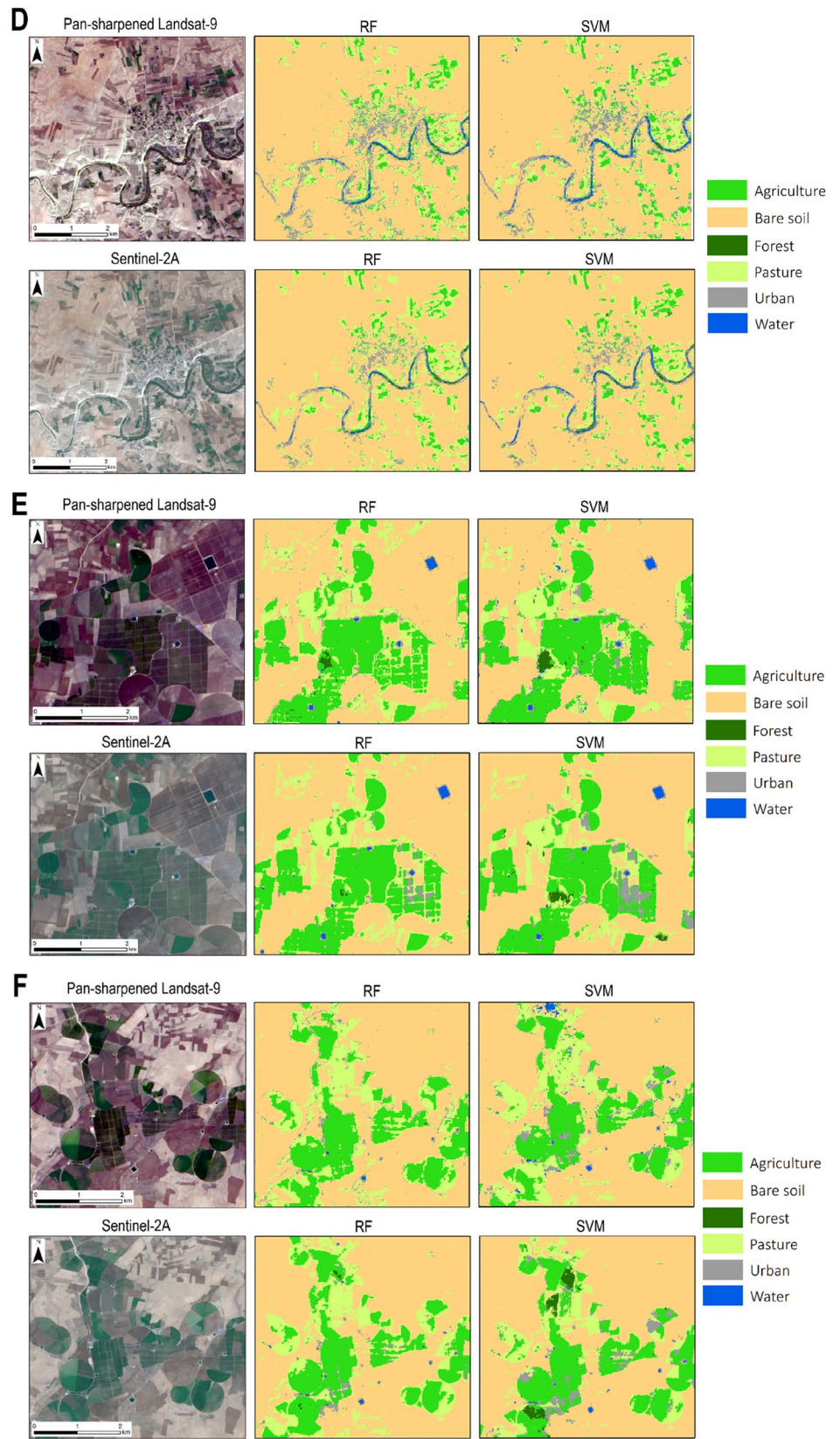
Fig. 8 (continued)

Table 3 The resulting precision, recall, and f1 score values for different classification combinations

	Pan-sharpened Landsat-9/RF			Pan-sharpened Landsat-9/SVM			Sentinel-2A/RF			Sentinel-2A/SVM		
	Precision	Recall	f1 score	Precision	Recall	f1 score	Precision	Recall	f1 score	Precision	Recall	f1 score
Agriculture	0.80	1.00	0.89	0.88	0.97	0.92	0.85	0.98	0.91	0.97	0.98	0.98
Bare soil	0.88	0.98	0.93	0.88	0.98	0.92	0.87	0.99	0.93	0.88	0.98	0.92
Forest	0.85	0.74	0.79	0.88	0.77	0.82	0.96	0.76	0.85	0.97	0.84	0.90
Pasture	0.79	0.89	0.84	0.82	0.93	0.87	0.86	0.91	0.88	0.82	0.94	0.87
Urban	0.87	0.85	0.86	0.77	0.80	0.78	0.89	0.86	0.87	0.88	0.84	0.86
Water	1.00	0.67	0.80	0.97	0.71	0.82	1.00	0.89	0.94	1.00	0.89	0.94

Table 4 Confusion matrix for the pan-sharpened Landsat-9 with the RF predictions (columns) and reference samples (rows)

	Pan-sharpened Landsat-9/RF					
	Agriculture	Bare soil	Forest	Pasture	Urban	Water
Agriculture	100	0	18	2	0	5
Bare soil	0	98	0	7	6	0
Forest	0	0	74	0	0	13
Pasture	0	2	8	89	9	4
Urban	0	0	0	2	85	11
Water	0	0	0	0	0	67
					OA	0.855
					Kappa	0.826
					Macro-f1	0.85

Table 5 Confusion matrix for the pan-sharpened Landsat-9 with the SVM predictions (columns) and reference samples (rows)

	Pan-sharpened Landsat-9/SVM					
	Agriculture	Bare soil	Forest	Pasture	Urban	Water
Agriculture	97	0	11	0	0	2
Bare soil	0	98	0	1	13	0
Forest	0	0	77	0	0	11
Pasture	0	2	11	93	5	2
Urban	3	0	1	6	80	14
Water	0	0	0	0	2	71
					OA	0.86
					Kappa	0.832
					Macro-f1	0.86

Table 6 Confusion matrix for the Sentinel-2 with the RF predictions (columns) and reference samples (rows)

	Sentinel-2/RF					
	Agriculture	Bare soil	Forest	Pasture	Urban	Water
Agriculture	98	0	16	1	0	0
Bare soil	0	99	1	5	9	0
Forest	0	0	76	0	0	3
Pasture	2	1	7	91	5	0
Urban	0	0	0	3	86	8
Water	0	0	0	0	0	89
					OA	0.898
					Kappa	0.878
					Macro-f1	0.9

Table 7 Confusion matrix for the Sentinel-2 with the SVM predictions (columns) and reference samples (rows)

	Sentinel-2/SVM					
	Agriculture	Bare soil	Forest	Pasture	Urban	Water
Agriculture	98	0	2	1	0	0
Bare soil	0	98	0	1	12	1
Forest	0	0	84	0	1	2
Pasture	2	2	14	94	3	0
Urban	0	0	0	4	84	8
Water	0	0	0	0	0	89
					OA	0.912
					Kappa	0.894
					Macro-f1	0.91

Accuracy Assessment of Classification

Model performance was evaluated for each land-use class based on the f1 score, recall, precision (Table 3), and the confusion matrix results (Tables 4, 5, 6, and 7). Comparing classification results (Tables 4 and 5) of the pan-sharpened Landsat-9 image showed that the SVM classifier (OA = 0.86, Kappa = 0.832 and macro-averaged f1 score = 0.86) performed slightly better than RF (OA = 0.855, Kappa = 0.826, and macro-averaged f1 score = 0.85). RF (Table 4) classified agriculture better than SVM (Table 5), with 100 well-classified samples for RF against 97 for SVM and an f1 score slightly higher for SVM (0.92 versus 0.89 for RF). Both algorithms classified bare soil with the same level of accuracy, with an f1 score between 0.92 and 0.93. SVM performed better than RF for the other classes, including forest (f1 score of 0.82 for SVM, versus 0.79 for RF), pasture (f1 score of 0.87 for SVM, versus 0.84 for RF), and water (f1 score of 0.82 for SVM, versus 0.80 for RF). Generally, we reported confusion between forest and agriculture/pasture and between urban and bare soil/pasture. In addition, a high misclassification was observed for water, with many samples classified as urban, forest, pasture, or agriculture.

For the Sentinel-2 (Tables 3, 6, and 7), once again, the SVM (OA = 0.912, Kappa = 0.894, and macro-averaged f1 score = 0.90) performed better than RF (OA = 0.898, Kappa = 0.878, and macro-averaged f1 score = 0.91). Generally, SVM (Table 7) classified forest better than RF (Table 6), with 84 well-classified samples against 76 for RF and an f1 score of 0.90 for SVM against 0.85 for RF. Forest class was confused with agriculture (16 samples) and pasture (7 samples) for RF, whereas the confusion was more pronounced with pasture (14 samples misclassified) for SVM. It should also be noted that some pasture samples were misclassified as urban or bare soil, although the f1 score of the two classifiers is identical with values between 0.87 and 0.88. Similarly, it was observed that water was confused with urban or forest with an f1 score equal to 0.94 for both classifiers.

Based on previous results (OA, Kappa, macro-averaged f1 score) and model performance for each class (f1 score), it can be concluded that Sentinel-2 showed better results than the pan-sharpened Landsat-9 for both classifiers. The lowest result was obtained with pan-sharpened Landsat-9 + RF, while Sentinel-2 + SVM had the best performance.

Discussion

The current study is aimed at comparing the ability of the new product (Landsat-9) and Sentinel-2 to provide land-use maps using RF and SVM classifiers. The findings of this study will help choose the right combination (image/algorithm) for a better land-use classification. The Landsat-9 image was recently made available, which might prevent discussing the obtained results with other similar studies. However, since Landsat-9 and Landsat-8 have approximately the same characteristics, studies that have evaluated Landsat-8 data were considered for discussion purposes.

The visual and statistical comparisons of the classification results are different. Based on visual comparison, the RF model seemed to perform better than the SVM, given that several features were well identified. In contrast to the RF results, the general observation of SVM classification shows confusion between several land-use classes, like the confusion between agriculture/forest and pasture/bare soil or urban. The combination of the RF model and the Sentinel-2 gives the best result, and misclassification of several elements observed in the other combinations was not observed in this case. The Sentinel-2 + RF could identify the water with high efficiency, considering the other combinations classified the water basin as urban. This could be attributed to the fact that the basin (1.5 m deep) was not completely filled with water, thus, it being confused with the urban class. It should also be noted that all combinations could classify the water well despite the central basins' green color, which is generally caused by a symbiosis between aerobic bacteria and algae. These results align with Toosi

et al. (2019), who used different Landsat time-series and machine learning methods (e.g., least squares SVM radial, SVM linear, and regularized discriminant analysis) to detect mangrove cover in southern Iran. They conclude that the RF model performed better based on visual comparisons. In another study, Adugna et al. (2022) compared the SVM and RF classifiers for extensive area land cover mapping of Africa. They found that the RF model performed 3% higher than the SVM model.

Statistical validation of the classification results based on testing samples showed that both images successfully classified agriculture and bare soil with high performance. Water was the exception, and both classifiers found problems classifying water for the pan-sharpened Landsat-9 image. In contrast, the water classification results of the Sentinel-2 image are significantly better than that of Landsat-9, which could be explained by the spatial resolution difference between the two images. The statistical evaluation showed that the SVM model performed slightly better than the RF. Nevertheless, this finding is consistent with several other studies. Rahman et al. (2020) used RF and SVM algorithms and their combination to classify LULC in two regions, Bhola (rural) and Dhaka (urban), based on Landsat-8, Sentinel-2, and planet satellite images. Their results revealed that Sentinel-2 performed better compared to both other images. They also found that SVM is significantly better than RF and ensemble model techniques. In addition, Thanh Noi and Kappas (2017) examined the performances of three algorithms (RF, KNN, and SVM) for classifying Sentinel 2 data in the North of the Red River Delta, Vietnam. Results showed that SVM has the highest overall accuracy and produces the best LULC maps, followed by the RF and KNN algorithms. In another study, Rana and Suryanarayana (2020) tested the combination of principal component analysis (PCA) and three algorithms (MLC, RF, and SVM) to produce LULCs from a Sentinel-2 image. They noticed that combining PCA with the SVM model can give the best result than the other classifiers. In addition, Sonobe et al. (2018) used the Sentinel-2 to extract 82 different remote sensing indices for crop-type classification. The results showed that the SVM classifier performed well compared to RF (89.3 to 92.0% of OA), and a combination of SVM and RF led to a significant improvement with an OA of 90.2 to 92.2%.

Furthermore, several studies reported that sample number and location might explain the difference between the virtual and statistical comparison results. For example, Thanh Noi and Kappas (2017) showed the impact of sample size and design on the performance of models to produce LULC maps. They found that when the training sample size was sufficiently large, i.e., greater than 750 pixels/class or representing an area of approximately 0.25% of the overall search area, all classifiers used (RF, KNN, and SVM) revealed a similar high AO (greater than 93.85%). In addition, according to Belgiu et al. (2014), some variations may be related to the choice of classification features and the assignment of feature clusters to discrete hierarchical levels. The land cover type of a high-resolution pixel is more accurately identified than a low-resolution pixel since the latter generalizes the heterogeneous surroundings (Zhao et al. 2014).

Overall, the difference between the two classifiers (RF and SVM) is negligible. Despite the Landsat-9 resolution improvement using the pan-sharpening technique, the advantage of the Sentinel-2 image was still apparent. Also, the presence of many outliers in the Sentinel-2 data used for classification did not affect the algorithm's performance. In general, several previous studies have reported the superiority of Sentinel-2 images over Landsat-8 images. Along the same line, Nyamekye et al. (2021) examined the performance of RGB bands from 3 sources (unmanned aerial vehicle, Landsat-8 and Sentinel-2) for artisanal and small-scale mining mapping in Ghana. The results showed that Landsat-8 and UAV showed poor performance, while Sentinel-2 gave the best results (OA = 0.949 and Kappa = 0.94). In another study in China, Wang et al. (2021) tried to identify cotton areas using two multispectral images (Landsat-8 and Sentinel-2) and a hyperspectral image (Orbita). This comparison showed that Orbita and Sentinel-2 performed better than Landsat-8. Also, both images (Landsat-8 and Sentinel-2) were used by Htitiou et al. (2019) for crop classification in irrigated areas in Morocco. Results showed a higher performance of Sentinel-2 (OA of 0.93 and Kappa of 0.91) than Landsat-8 (OA and Kappa of 0.9 and 0.88, respectively).

Finally, the comparative analysis of this work and other similar studies had shown the superiority of Sentinel-2, despite attempts to improve the accuracy of Landsat-9 images. This difference can be attributed mainly to the higher spatial and spectral resolutions. Also, the three red-edge bands of Sentinel-2 have been shown in several studies to be very useful for improving the accuracy of vegetation maps and for also classification of a wide range of crops (Forkuor et al. 2018; Immitzer et al. 2016; Ramoelo et al. 2015).

Conclusion and Future Work

The present study evaluates two machine learning algorithms (RF and SVM) for land-use mapping, using two of the most popular and commonly used satellite image sources, the recently launched Landsat-9 and Sentinel-2. The potential to improve the performance of Landsat-9 has also been tested by pan-sharpening the different bands for high-resolution data (15 m). For optimal performance of the two classifiers, a model tuning approach was applied by trying

different combinations of the critical parameters for each model. The results showed that the SVM performed slightly better than RF. Furthermore, the Sentinel-2 demonstrated significant capabilities for multiple-variety classification compared to Landsat-9, despite the improved resolution of the latter.

Overall, this study represents a first attempt to evaluate the capabilities of Landsat-9 to generate accurate land-use maps. This study opens the path for future works, such as crop-type classification using phenological information derived from multispectral or hyperspectral images; testing other machine learning or deep learning classifiers to optimize performance and processing time. In addition, other methods of pan-sharpening algorithms or alternative data sources can be tested to improve the Landsat-9 resolution.

Declarations

Ethics Approval and Consent to Participate This article does not contain any study conducted by any of the authors that would require ethical approval.

This article does not contain any studies involving human participants performed by any of the authors.

Consent for Publication All authors have consented to submission and publication in the Journal of *Geovisualization and Spatial Analysis*.

Conflict of Interest The authors declare no competing interests.

References

Adugna T, Xu W, Fan J (2022) Comparison of random forest and support vector machine classifiers for regional land cover mapping using coarse resolution FY-3C images. Remote Sensing 14(3):574

Alshari EA, Gawali BW (2021) Development of classification system for LULC using remote sensing and GIS. Glob Transit Proc 2(1):8–17

Aouichaty N, Bouslihim Y, Hilali S, Zouhri A, Koulali Y (2022) Estimation of water erosion in abandoned quarries sites using the combination of RUSLE model and geostatistical method. Sci Afr 16:e01153

Atkinson PM (2013) Downscaling in remote sensing. Int J Appl Earth Obs Geoinf 22:106–114

Belgiu M, Drăguţ L, Strobl J (2014) Quantitative evaluation of variations in rule-based classifications of land cover in urban neighbourhoods using WorldView-2 imagery. ISPRS J Photogramm Remote Sens 87:205–215. https://doi.org/10.1016/j.isprsjprs.2013.11.007

Berihun ML, Tsunekawa A, Haregeweyn N, Tsubo M, Fenta AA (2021) Changes in ecosystem service values strongly influenced by human activities in contrasting agro-ecological environments. Ecol Process 10(1):1–18

Bouslihim Y, Rochdi A, Paaza NEA (2021) Machine learning approaches for the prediction of soil aggregate stability. Heliyon 7(3):e06480

Bouslihim Y, Rochdi A, Aboutayeb R, El Amrani-Paaza N, Miftah A, Hssaini L (2021) Soil aggregate stability mapping using remote sensing and GIS-based machine learning technique. Front Earth Sci 9:1–13

Breiman L (2001) Random forests. Mach Learn 45(1):5–32

Crabbe RA, Lamb D, Edwards C (2020) Discrimination of species composition types of a grazed pasture landscape using Sentinel-1 and Sentinel-2 data. Int J Appl Earth Obs Geoinf 84:101978

Du P, Bai X, Tan K, Xue Z, Samat A, Xia J, Liu W (2020) Advances of four machine learning methods for spatial data handling: a review. J Geovisualization Spat Anal 4(1):1–25

Forkuor G, Dimobe K, Serme I, Tondoh JE (2018) Landsat-8 vs. Sentinel-2: examining the added value of sentinel-2's red-edge bands to land-use and land-cover mapping in Burkina Faso. GIScience remote sens 55(3):331–354

Fu B, Liu M, He H, Lan F, He X, Liu L, Huang L, Fan D, Zhao M, Jia Z (2021) Comparison of optimized object-based RF-DT algorithm and SegNet algorithm for classifying karst wetland vegetation communities using ultra-high spatial resolution UAV data. Int J Appl Earth Obs Geoinf 104:102553

Georganos S, Grippa T, Lennert M, Vanhuysse S, Johnson BA, Wolff E (2018) Scale matters: spatially partitioned unsupervised segmentation parameter optimization for large and heterogeneous satellite images. Remote Sens 10(9):1440

Ghasemloo N, Matkan AA, Alimohammadi A, Aghighi H, Mirbagheri B (2022) Estimating the agricultural farm soil moisture using spectral indices of Landsat 8, and Sentinel-1, and artificial neural networks. J Geovisualization Spat Anal 6(2):1–12

Ghayour L, Neshat A, Paryani S, Shahabi H, Shirzadi A, Chen W, Al-Ansari N, Geertsema M, Pourmehdi Amiri M, Gholamnia M, Dou J, Ahmad A (2021) Performance evaluation of Sentinel-2 and Landsat 8 OLI data for land cover/use classification using a comparison between machine learning algorithms. Remote Sens 13(7):1349

Gillespie AR, Kahle AB, Walker RE (1987) Color enhancement of highly correlated images. II. Channel ratio and "chromaticity" transformation techniques. Remote Sens Environ 22(3):343–365

Goel RK, Yadav CS, Vishnoi S, Rastogi R (2021) Smart agriculture–urgent need of the day in developing countries. Sustain Comput: Informa Syst 30:100512

Hargreaves PK, Watmough GR (2021) Satellite Earth observation to support sustainable rural development. Int J Appl Earth Obs Geoinf 103:102466

Htitiou A, Boudhar A, Lebrini Y, Hadria R, Lionboui H, Elmansouri L, Tychon B, Benabdelouahab T (2019) The performance of random forest classification based on phenological metrics derived from Sentinel-2 and Landsat 8 to map crop cover in an irrigated semi-arid region. Remote Sens Earth Syst Sci 2(4):208–224

Huyck C, Verrucci E, Bevington J (2014) Remote sensing for disaster response. In: Shroder JF, Wyss M (eds) Earthquake hazard, risk and disasters. Elsevier, Amsterdam. https://doi.org/10.1016/B978-0-12-394848-9.00001-8

Ibrahim E, Barnabé P, Ramanaidou E, Pirard E (2018) Mapping mineral chemistry of a lateritic outcrop in new Caledonia through generalized regression using Sentinel-2 and field reflectance spectra. Int J Appl Earth Obs Geoinf 73:653–665

Immitzer M, Vuolo F, Atzberger C (2016) First experience with Sentinel-2 data for crop and tree species classifications in central Europe. Remote Sens 8(3):166. https://doi.org/10.3390/rs8030166

John K, Bouslihim Y, Bouasria A, Razouk R, Hssaini L, Isong IA, Ait M'barek S, Ayito EO, Ambrose-Igho G (2022) Assessing the impact of sampling strategy in random forest-based predicting of soil nutrients: a study case from Northern Morocco. Geocarto Int 1–14. https://doi.org/10.1080/10106049.2022.2048091

Johnson BA, Tateishi R, Hoan NT (2012) Satellite image pansharpening using a hybrid approach for object-based image analysis. ISPRS Int J Geo Inf 1(3):228–241

Kala AK, Kumar M (2022) Role of geospatial technologies in natural resource management. In: Climate impacts on sustainable natural resource management. Wiley Blackwell, Chichester

Karan SK, Samadder SR (2018) A comparison of different land-use classification techniques for accurate monitoring of degraded coal-mining areas. Environ Earth Sci 77(20):1–15

Kollert A, Bremer M, Löw M, Rutzinger M (2021) Exploring the potential of land surface phenology and seasonal cloud free composites of one year of Sentinel-2 imagery for tree species mapping in a mountainous region. Int J Appl Earth Obs Geoinf 94:102208

Lary DJ, Zewdie GK, Liu X et al (2018) Machine learning applications for earth observation. Earth observation open science and innovation. Springer, Cham, pp 165–218. https://doi.org/10.1007/978-3-319-65633-5

Liu JG, Moore JM (1998) Pixel block intensity modulation: Adding spatial detail to TM band 6 thermal imagery. Int J Remote Sens 19(13):2477–2491

Meyer D, Wien FT (2015) Support vector machines. Interface libsvm packag e1071:28

Montalván-Burbano N, Velastegui-Montoya A, Gurumendi-Noriega M, Morante-Carballo F, Adami M (2021) Worldwide research on land use and land cover in the Amazon Region. Sustainability 13(11):6039

Nagne AD, Vibhute AD, Dhumal RK, Kale KV, Mehrotra SC (2019) Urban LULC change detection and mapping spatial variations of Aurangabad City using IRS LISS-III Temporal datasets and supervised classification approach. Data Analytics and Learning 43:369–386. https://doi.org/10.1007/978-981-13-2514-4_31

Nyamekye C, Ghansah B, Agyapong E, Obuobie E, Awuah A, Kwofie S (2021) Examining the performances of true color RGB bands from Landsat-8, Sentinel-2 and UAV as stand-alone data for mapping artisanal and small-scale mining (ASM). Remote Sens Appl: Soc Environ 24:100655

Rahman A, Abdullah HM, Tanzir MT, Hossain MJ, Khan BM, Miah MG, Islam I (2020) Performance of different machine learning algorithms on satellite image classification in rural and urban setup. Remote Sens Appl: Soc Environ 20:100410

Ramoelo A, Cho M, Mathieu R, Skidmore AK (2015) Potential of Sentinel-2 spectral configuration to assess rangeland quality. J Appl Remote Sens 9(1):094096

Rana VK, Suryanarayana TMV (2020) Performance evaluation of MLE, RF and SVM classification algorithms for watershed scale land use/land cover mapping using sentinel 2 bands. Remote Sens Appl: Soc Environ 19:100351

Shaharum NSN, Shafri HZM, Gambo J, Abidin FAZ (2018) Mapping of Krau Wildlife Reserve (KWR) protected area using Landsat 8 and supervised classification algorithms. Remote Sens Appl: Soc Environ 10:24–35

Sonobe R, Yamaya Y, Tani H, Wang X, Kobayashi N, Mochizuki KI (2018) Crop classification from Sentinel-2-derived vegetation indices using ensemble learning. J Appl Remote Sens 12(2):026019

Talukdar S, Singha P, Mahato S, Pal S, Liou YA, Rahman A (2020) Land-use land-cover classification by machine learning classifiers for satellite observations—a review. Remote Sens 12(7):1135

Thanh Noi P, Kappas M (2017) Comparison of random forest, k-nearest neighbor, and support vector machine classifiers for land cover classification using Sentinel-2 imagery. Sensors 18(1):18

Toosi NB, Soffianian AR, Fakheran S, Pourmanafi S, Ginzler C, Waser LT (2019) Comparing different classification algorithms for monitoring mangrove cover changes in southern Iran. Glob Ecol Conserv 19:e00662

U.S. Geological Survey (2019) Landsat 9 (ver. 1.3, August 2022): U.S. Geological Survey Fact Sheet 2019–3008, 2 p. https://doi.org/10.3133/fs20193008

Van Leeuwen B, Tobak Z, Kovács F (2020) Machine learning techniques for land use/land cover classification of medium resolution optical satellite imagery focusing on temporary inundated areas. J Environ Geogr 13(1–2):43–52

Wang C, Chen Q, Fan H, Yao C, Sun X, Chan J, Deng J (2021) Evaluating satellite hyperspectral (Orbita) and multispectral (Landsat 8 and Sentinel-2) imagery for identifying cotton acreage. Int J Remote Sens 42(11):4042–4063

Wang Z, Ziou D, Armenakis C, Li D, Li Q (2005) A comparative analysis of image fusion methods. IEEE Trans Geosci Remote Sens 43(6):1391–1402

Zhang Y (1999) A new merging method and its spectral and spatial effects. Int J Remote Sens 20(10):2003–2014

Zhao Y, Gong P, Yu L, Hu L, Li X, Li C, Zhang H, Zheng Y, Wang J, Zhao Y, Cheng Q, Liu C, Liu S, Wang X (2014) Towards a common validation sample set for global land-cover mapping. Int J Remote Sens 35(13):4795–4814